Atmos. Chem. Phys. Discuss., doi:10.5194/acp-2016-390, 2016
Manuscript under review for journal Atmos. Chem. Phys.
Published: 13 May 2016

Atmospheric Chemistry and Physics Discussions

Properties of aerosols and formation mechanisms over southern China during the monsoon season

Weihua Chen[1], Xuemei Wang[2]*, Jason Blake Cohen[3], Shengzhen Zhou[2*], Zhisheng Zhang[4], Ming Chang[1], and Chuen Yu Chan[5]

[1] *School of Environmental Science and Engineering, Sun Yat-Sen University, Guangzhou, China*

[2] *School of Atmospheric Sciences, Sun Yat-Sen University, Guangzhou, China*

[3]*Department of Civil and Environmental Engineering, National University of Singapore, Singapore*

[4] *South China Institute of Environmental Sciences, Guangzhou, China*

[5]*Key Laboratory of Aerosol, SKLLQG, Institute of Earth Environment, Chinese Academy of Sciences, Xi'an, China*

[*]Corresponding author:
Xuemei Wang (eeswxm@mail.sysu.edu.cn)
Shengzhen Zhou (zszking@126.com)

Atmos. Chem. Phys. Discuss., doi:10.5194/acp-2016-390, 2016
Manuscript under review for journal Atmos. Chem. Phys.
Published: 13 May 2016

Atmospheric Chemistry and Physics Discussions

Abstract

Measurements of size-resolved aerosols from 0.25 to 18 μm were conducted at three sites (urban, suburban and background sites) and used in tandem with an atmospheric transport model to study the size distribution and formation of atmospheric aerosols in southern China during the monsoon season (May-June) in 2010. The mass distribution showed the majority of chemical components were found in the smaller size bins (<2.5 μm). Sulfate, was found to be strongly correlated with aerosol water, and anti-correlated with atmospheric SO_2, hinting at aqueous-phase reactions being the main formation pathway. Nitrate was the only major species that showed a bi-modal distribution at the urban site, and was dominated by the coarse mode in the other two sites, suggesting that an important component of nitrate formation is chloride depletion of sea salt transported from the South China Sea. In addition to these aqueous-phase reactions and interactions with sea salt aerosols, new particle formation, chemical aging, and long-range transport from upwind urban or biomass burning regions were also found to be important in at least some of the sights on some of the days. This work therefore summarizes the different mechanisms that significantly impact the aerosol chemical composition during the Monsoon over southern China.

Keywords: chemical component, mass size distribution, aqueous-phase reaction chloride depletion

Atmos. Chem. Phys. Discuss., doi:10.5194/acp-2016-390, 2016
Manuscript under review for journal Atmos. Chem. Phys.
Published: 13 May 2016

Atmospheric Chemistry and Physics Discussions

1. Introduction

Atmospheric aerosols are solid and liquid substances ubiquitously suspended in the Earth's atmosphere, that impair visibility, negatively affect human health, and directly and indirectly impact regional and global climate (Chung and Seinfeld, 2005; Cohen et al., 2011; Jacobson, 2001; Kim et al., 2008; Ramanathan and Carmichael, 2008; Rosenfeld et al., 2014; Tao et al., 2009; Burnett et al., 2014). The size distributions and chemical composition of aerosols play essential roles on their transport, transformation, removal mechanisms (Seinfeld and Pandis, 2006; Zhao and Gao, 2008a; Giglio et al., 2003, 2006; Cohen and Wang, 2013; Petrenko, et al., 2012; Cohen and Prinn, 2011; Delene and Ogren, 2002; Dubovik et al., 2000). And also, to some extent, they provide useful information to validate and improve model performance (Pillai and Moorthy, 2001; Cohen and Wang, 2013; Myhre et al., 2013; Schuster et al., 2006; Tsigaridis et al., 2014; Cohen and Lecoeur, 2015; Cohen, 2014; Cohen and Wang 2013). In the environment, the most important aerosol processes occur over the aitken, condensation, droplet, and coarse size modes, where new particles form in the condensation mode, and in-cloud processing and aqueous reactions occur in the droplet mode (Yao et al, 2003a; Meng and Seinfeld, 1994; Wang et al., 2012; Volkamer et al., 2009; Lim et al., 2010; Ervens et al., 2011). On the other hand, coarse mode aerosols are usually due to different source types and therefore provide further information about the aerosol distribution at a given location.

Previous research suggests that sulfate is mostly contained in the non-coarse

Atmos. Chem. Phys. Discuss., doi:10.5194/acp-2016-390, 2016
Manuscript under review for journal Atmos. Chem. Phys.
Published: 13 May 2016

Atmospheric Chemistry and Physics Discussions

modes, with the conversion of SO_2 occurring mostly via gas-phase oxidation followed by condensation, or through droplet mode sulfate produced from fog/cloud process (Meng and Seinfeld, 1994; Barth et al., 1992). On the other hand, nitrate usually has a bi-modal distribution with peaks in both the fine and coarse modes. Fine mode nitrate is formed mainly by oxidation of NO_2 to HNO_3 and subsequent condensation, or from the heterogeneous hydrolysis of N_2O_5, while coarse mode nitrate is often observed due to the effect of chloride depletion of sea salt aerosols (Pierson and Brachaczek, 1988; Harrison and Pio, 1983). Ammonium is mostly found in the fine mode and is chemically associated with sulfate and nitrate. Carbonaceous materials, organic carbon (OC) and elemental carbon (EC), are both found primarily in the non-coarse mode. While both OC and EC are impacted by differing emissions sources and wet deposition, there are other significant differences: EC is hydrophobic and radiatively active, while OC is hydrophylic and further has significant source terms from condensation and secondary particle formation (Lan et al., 2011).

Meteorological conditions also play a vital role in the size distribution and the formation of secondary aerosols. Southern China has high relative humidity and temperature, leading to significant aerosol water uptake and secondary aerosol formation and processing. Furthermore, during the Monsoon period, South China is greatly affected by air masses transported from the South China Sea, leading to a large variation in the upwind aerosol compositions and loadings as compared to those from local or continental sources.

In this paper, we present a unique database of the size-different mass distribution

Atmos. Chem. Phys. Discuss., doi:10.5194/acp-2016-390, 2016
Manuscript under review for journal Atmos. Chem. Phys.
Published: 13 May 2016

of sulfate, nitrate, ammonium and carbonaceous aerosols during the Monsoon Season over southern China. The data is sampled from a combination of three different sites, one in an urban area, one in a suburban area, and one in a remote area, providing further insights into the characteristics in each of these regions. The measurements made during the observation periods were analyzed in tandem with each other and a meteorological model, leading to some robust conclusions regarding the formation mechanisms of water soluble ions, the identification and impacts of long-range transport of biomass and urban sources, and the impacts mixing sea-salt and urban pollutants.

2. Measurements and methodology

2.1. Description of the sampling sites

The field study was conducted at three sites in southern China (Figure 1), two of which were situated in Guangdong and the other in Hainan. Guangdong is located in a subtropical monsoon climate, primarily influenced by cold and dry air masses from the North in December to February, and warm and wet air masses from the South China Sea in May to August. It has a single annual local rainy season extending from April to September. Hainan is located further to the south, and has year-round warm to hot weather and a distinct rainy season from May to October.

The first site was set at (23.12 °N, 113.36 °E), on the rooftop of a building in the South China Institute of Environmental Sciences, Guangzhou (GZ), an urban mega-city containing more than 13 million people. The site was located about 50m

Atmos. Chem. Phys. Discuss., doi:10.5194/acp-2016-390, 2016
Manuscript under review for journal Atmos. Chem. Phys.
Published: 13 May 2016

Atmospheric Chemistry and Physics Discussions

above ground, in an area surrounded by residential and commercial buildings, with the nearest arterial roads located about 200m away. There were no significant industrial emission sources found around the site. This site was chosen since it is highly representative of a typical megacity.

The second site was located at (22.34 °N, 113.58 °E), on the rooftop of the library at Sun Yat-Sen University, in the city of Zhuhai (ZH), a medium sized city of about 1.6 million people located in Southern Guangdong adjacents to Macau. The site was located about 60m above the ground, in an area surrounded by mountains on three sides and the estuary where the Pearl River meets the South China Sea about 500m away on the fourth side. There are no significant industrial or major transportation emissions sources nearby. This site was chosen since it is highly representative of a coastal partially urbanized area.

The third site was located at Jianfeng Mountain (JFM, 18.74 °N, 108.86 °E), in a tropical rainforest situated at the Southwest corner of Hainan. This site is distant from the major cities of Hainan province and is further located about 5km away from the coast. JFM is not directly influenced by anthropogenic emissions and is generally regarded as a background site to investigate the long-rang transport (Zhang et al., 2013a). This site was chosen both because it is representative of a remote site and because it receives air masses from three different directions: continental East Asia to the North, the South China Sea to the South, and Southeast Asia to the West.

2.2 Sampling of aerosol

Atmos. Chem. Phys. Discuss., doi:10.5194/acp-2016-390, 2016
Manuscript under review for journal Atmos. Chem. Phys.
Published: 13 May 2016

Atmospheric Chemistry and Physics Discussions

The sampling campaign was performed in May and June 2010. To attain size-segregated particle samples, a 6-stage High Flow Impactor (MSP) with an airflow rate of 100 L min^{-1} was employed, with cutoff diameters (D_p) of 18, 10, 2.5, 1.4, 1.0, 0.44 and 0.25 μm. A total of 6 sets of size-segregated particle samples were collected on 77 mm and 90 mm (for inlet) quartz microfiber filters (Pall Corporation, NY, USA). 24h sampling was performed every other day in GZ and ZH, while 48h sampling was conducted every day in JFM. Over the entire duration of the campaign, there were 70 samples taken in GZ, 56 samples taken in ZH, and 140 samples taken in JFM. Detailed information of the aerosol sampling and in-lab chemical analytical techniques can be found in Zhang et al. (2013a).

To be consistent with the background literature and the constraints of the size bins measured in this study, we implement 2.5 μm as the cut-off size to separate fine and coarse particles, and the size bins from 0.44-1.4 μm to define droplet particles.

Although we were not able to directly measure aerosol water content, given its importance for the study here, we instead to estimate the amount by the use of AIM-II model (Clegg et al., 1998). Implementation of the model required the use of measured molar concentrations of sulfate [SO_4^{2-}], nitrate [NO_3^-], ammonium [NH_4^+], ambient temperature (T), and relative humidity (RH). Further, an approximation of the particle strong acidity $[H^+]_s$. is required, which also has been computed from measurements following Eq. (1).

$$\left[H^+\right]_s = 2\left[SO4^{2-}\right] + \left[NO_3^-\right] - \left[NH_4^+\right] \quad (1)$$

Atmos. Chem. Phys. Discuss., doi:10.5194/acp-2016-390, 2016
Manuscript under review for journal Atmos. Chem. Phys.
Published: 13 May 2016

Atmospheric Chemistry and Physics Discussions

157 **2.3 Meteorological data**

158 Meteorological parameters, including wind speed (WS), wind direction (WD),
159 temperature (T), relative humidity (RH), pressure (P), and precipitation were
160 simultaneously monitored in GZ and JFM sites with a time resolution of 30 minutes.
161 The same meteorological parameters in ZH, as well as the daily low-level cloud cover
162 data at all three sites, were obtained from the China Meteorological Data Sharing
163 Service System (http://data.cma.cn/site/index.html).

164

165 **2.4 Remotely sensed measurements**

166 Aerosol optical depth (AOD), Fire Radiative Power (FRP), and Fire Quality
167 Assurance [QA] data were obtained from the MODIS sensors aboard both the AQUA
168 and TERRA satellites. Specifically, we obtained the Collection 6, 3km Level 2 swath
169 product for AOD [Remer et al., 2013], and Collection 5.1, 1km Level 2 swath
170 products for FRP and QA[Giglio et al., 2006]. All of the data is cloud-screened, with
171 AOD data being computed using different algorithms over land and water, and the fire
172 data using 19 different channels for quality assurance. We only accept values for FRP
173 and Fire Count where the QA is at least 90%.

174

175 **2.5 Atmospheric transport model**

176 Two Lagrangian particle dispersion models, the Hybrid Single Particle Lagrangian
177 Integrated Trajectory (HYSPLIT) (Draxler and Hes, 1998) and FLEXPART coupled
178 with The Weather and Research and Forecasting (WRF) model were used to compute

Atmos. Chem. Phys. Discuss., doi:10.5194/acp-2016-390, 2016
Manuscript under review for journal Atmos. Chem. Phys.
Published: 13 May 2016

Atmospheric Chemistry and Physics Discussions

air parcel trajectories (Stohl et al., 1998; Brioude et al., 2013). HYSPLIT uses single air parcels to compute trajectories with the use of Global Data Assimilation System (GDAS, 1 °×1 °) as input data. FLEXPART, on the other hand, uses a larger number of air parcels to compute trajectories based on the meteorological predictions provided by mesoscale model WRF

An Eulerian model, WRF/Chem V3.4.1 was used in this study to simulate fog processing. For this mode, the target region's was modeled at a spatial resolution of 3 ×3km. Detail information about the WRF/Chem model set-up refers to Situ et al. (2013). While WRF was used to simulate the meteorological fields required for the FLEXPART back trajectory calculations over the larger region. In this case, the region was modeled with a spatial resolution of 27×27 km and a temporal resolution of 1 hour.

3. Results and discussion

3.1. Overall aerosol characteristics

The mass time series of the total aerosol mass (PM_{10}) at the three sites has an average and standard deviation of 46.7±20.6, 23.7±7.3, and 8.0±2.6 μg m^{-3} in GZ, ZH, and JFM respectively (Figure S1). The mean and range of PM_{10} in highly urban GZ was both higher and wider than in suburban ZH and rural JFM, with the respective ranges being [22.5, 92.3], [12.9, 34.6], and [4.6, 14.2] μg m^{-3} in the three sites. In terms of the mass size distribution, the percentage of $PM_{1.0}$ to PM_{10} and $PM_{2.5}$ to PM_{10} fell within the range of [0.52, 0.55] and [0.72, 0.76] respectively (Table 1).

Atmos. Chem. Phys. Discuss., doi:10.5194/acp-2016-390, 2016
Manuscript under review for journal Atmos. Chem. Phys.
Published: 13 May 2016

Atmospheric Chemistry and Physics Discussions

When considered as a whole, it is the smaller sized particles that dominate the aerosol loading at all three of these sites.

Looking at the data on a species-by-species level, the majority of individual chemical species contribute at least 57% to $PM_{2.5}$. The sole exception is nitrate at ZH and JFM, which were mainly concentrated in the coarse mode with a percentage of above 90%. Overall, the sum of five major chemical components (i.e. sulfate, nitrate, ammonium, OC, and EC) accounted for about 90% of the total mass concentration of detected chemical components across all three sites.

Two of the species, sulfate and OC, were found to dominate particle composition, with concentration of 11.7 ±5.2, 8.8 ±3.2, 2.2 ±1.5 μg m^{-3} for sulfate and 7.2 ±2.7, 3.0 ±1.5, 1.8 ±0.8 μg m^{-3} for OC in GZ, ZH and JFM, respectively. Sulfate concentration was much higher than that of OC in urban and suburban locations no matter what the particle size was, while OC concentration was similar to that of sulfate in fine particles and slightly higher in coarse particles at the remote site. These findings are consistent with the nature of the sources of sulfur from industrial and shipping sources.

Nitrate, although primarily formed similar sources as sulfate, such as mobile vehicles and high temperature industry, showed a remarkable difference between urban and background site, with ranging from fourteen to thirty times higher in GZ than in the other sites, especially for fine mode nitrate. This is consistent with its more rapid oxidation of its precursor species, especially so in the urban atmosphere (Cohen et al., 2011). Furthermore, it was found to have a relatively insignificant concentration

Atmos. Chem. Phys. Discuss., doi:10.5194/acp-2016-390, 2016
Manuscript under review for journal Atmos. Chem. Phys.
Published: 13 May 2016

Atmospheric Chemistry and Physics Discussions

in ZH and JFM, indicating far less anthropogenic emission of the precursor over these two sites.

The values of OC and EC in $PM_{2.5}$ were 7.2 ±2.7 and 3.4 ±3.2 μg m^{-3} in GZ, 3.0 ±1.5 and 1.5 ±0.9 μg m^{-3} in ZH. These values were lower than that of found in previous studies done in GZ and ZH during the wet season: OC and EC were 13.1 and 4.6 μg m^{3} in GZ in 2007, 14.8 and 8.1 μg m^{-3} in GZ in 2002, and 5.4 and 1.9 μg m^{-3} in ZH in 2002 (Cao et al., 2004; Tao et al., 2009). Furthermore, OC and EC concentrations in JFM were found to be lower than that at other forest sites in China, such as Hengshan: 3.01 and 0.54 μg m^{-3} in 2009 (Zhou et al., 2012), Daihai: 8.1 and 1.81 μg m^{-3} in 2007 (Han et al., 2008), and Taishan: 6.07 and 1.77 μg m^{-3} in 2007 (Wang et al., 2011). However, the EC and OC in JFM were similar to some background sites in other countries, such as Puy De Dome in France: 2.4 and 0.26 μg m^{-3} in 2004 (Pio et al., 2007) and Sonnblick in Austria: 1.38 and 0.23 μg m^{-3} in 2003 (Pio et al., 2007). This finding is not unexpected, since there are very few urban sources near the site. It is therefore relatively representative of a remote background site, and will be treated as such subsequently in this paper.

3.2. Size distribution by chemical composition

The mass size distribution of major compositions at the three sites during the study period, showing that sulfate had a single-peaked distribution, with the maximum value found in the 0.44-1.0 μm size over all sites and under all different meteorological conditions examined in this study. The droplet mode sulfate was about

Atmos. Chem. Phys. Discuss., doi:10.5194/acp-2016-390, 2016
Manuscript under review for journal Atmos. Chem. Phys.
Published: 13 May 2016

Atmospheric Chemistry and Physics Discussions

56.0 ±8.0 %, 63.5 ±5.1 % and 58.8 ±9.4 % of the total sulfate mass in GZ, ZH and JFM, respectively (Figure 2). This confirms that secondary processing is essential, with aqueous-phase reactions playing a crucial role on the formation and/or growth of droplet sulfate, throughout all of these different regions. It is interesting to note that ZH had the highest relative concentration of droplet model sulfate, which although it is less urban than GZ, is consistent with the fact that it is located very close to large amounts of sulfur emissions from the shipping traffic at the massive nearby ports of Hong Kong and Shenzhen.

Droplet mode ammonium was mainly due to ammonia vapor that reacted with or condensed on an acidic particle surface. Ammonia was observed to highly correlate with sulfate at the three sites ($R>0.81$, $P<0.01$), particularly so in the size range of 0.44-1.0 μm. This is consistent with the fact that sulfuric acid preferentially reacts with ammonia (Zhuang et al., 1999), and that most of sulfate in the atmosphere is generally found as ammonium sulfate in the droplet mode (Liu et al., 2008; Zhuang et al., 1999).

The nitrate size distribution was found to be bi-modal in GZ, with the peaks occurring in the 0.44-1.0 μm and 2.5-10 μm size ranges. However, it was found that the majority of nitrate was found in the fine mode particles when the air came from continental sources with the percentage of 33%, and conversely it was found in the coarse mode particles when the air came from an oceanic source with the percentage of 51%. This is consistent with the fact that droplet mode nitrate is formed similarly to sulfate, after oxidation of the NOx, but is only converted into aerosol after all of the

Atmos. Chem. Phys. Discuss., doi:10.5194/acp-2016-390, 2016
Manuscript under review for journal Atmos. Chem. Phys.
Published: 13 May 2016

Atmospheric Chemistry and Physics Discussions

sulfate first reacts, and only in the presence of sufficient ammonia (Zhuang et al., 1999). On the other hand, this result is consistent with the fact that nitrate was found mostly in the coarse mode in ZH and JFM, where it accounted for up to 40% of total particulate mass. A higher relative humidity, consistent with the warm and wet atmosphere over the South China Sea, makes gaseous nitric acid more likely to be absorbed by coarse particles in the atmosphere (Anlauf et al., 2006), resulting in a higher relative concentration of nitrate in the coarse mode in ZH and JFM (where the relative humidity averaged 80 and 91% respectively, as compared to only 73% in GZ). Further, the presence of coarse mode nitrate is consistent with chlorine reduction, as talked about later.

OC and EC showed a similar mono-modal distribution in GZ and ZH, with a dominant and broad peak over the range from 0.25-1.4 μm. On the other hand, a bi-modal distribution was found in JFM. In urban and suburban areas, there are significant primary sources from traffic and industry in the e.g. Huang et al. (2006) and Cao et al. (2004). It is also consistent with the high levels emissions due to the ship traffic to Shenzhen and Hong Kong, both of which are located near ZH, which in turn would compensate for the otherwise reduced industrial and traffic sources. OC has both primary sources, which are similar to those for EC as well as secondary formation. There were a few days in which the ratios of OC to EC are not consistent, indicating a large secondary source of OC. We investigate these days and find that long-range transported of far-upwind urbanization and biomass burning is responsible, as talked about later. Additionally, there is some coarse mode OC present in JFM,

Atmos. Chem. Phys. Discuss., doi:10.5194/acp-2016-390, 2016
Manuscript under review for journal Atmos. Chem. Phys.
Published: 13 May 2016

suggesting a possible source of biological aerosol, which is consistent with the large amounts of vegetation present in that region.

3.3. Observed Aqueous-phase reaction of droplet mode sulfate

The daily droplet mode sulfate ranged from 3.0-13.6, 1.6-9.5 and 0.5-4.9 μg m^{-3} in GZ, ZH and JFM respectively. The cases with concentration of droplet sulfate above the mean plus one standard deviation (8^{th} and 12^{th} May in GZ, 12^{th} May and 1^{st} Jun. in ZH, and 4^{th} and 13^{th} May 2010 in JFM) were chosen to investigate the effect of aqueous-phase reaction in the formation of droplet mode sulfate (blue shade in Figure S1). In each of these cases, it was found that droplet mode sulfate accounted for about two thirds of the total mass concentration of sulfate at the three sites, indicating that the average size was small and that the particles were therefore relatively young, strongly indicative of new particle formation.

A backward trajectory analysis found that during these events, the air masses at these sites mainly originated over the South China Sea (figures not show here). Additionally, it was determined that during these times at the sites there was an abnormally high amount of low cloud cover 60-70% and a relatively higher relative humidity (75~83%) (Table 2). This combination is consistent with moist air being transported over land where ship and industrial SO_2 emissions can undergo chemistry in the presence of large amounts of liquid cloud water, to form droplet-model sulfate.

We estimated the liquid water content using the AIM-II model (Equation 1). The results showed a significant correlation with droplet mode sulfate in GZ (R=0.98,

Atmos. Chem. Phys. Discuss., doi:10.5194/acp-2016-390, 2016
Manuscript under review for journal Atmos. Chem. Phys.
Published: 13 May 2016

311 P<0.05), ZH (R=0.53, P<0.05) and JFM (R=0.80, P<0.05), indicating that water
312 content correlated closely with the sulfate aerosol loadings. This is further evidence
313 that aqueous formation was likely an important contributing factor.
314 We further investigated the aqueous-phase reaction of particles due to fog
315 processing for the data from 8th May in GZ. This is because the measured visibility
316 met the World Meteorological Organization cutoff value of less than 1 km due to
317 water droplets, in the early morning (05:00-07:00 LT) (Figure 3(c)). Consistently,
318 during this time, it was found that the relatively humidity was quite high (RH>90%)
319 and the wind was quite low (wind speeds<1.0 m s^{-1}). Also during this time, the cloud
320 fraction and simulated 2m relative humidity were up to 90% over Southern China
321 (Figure 3(a-b)). Furthermore, the depression dew point (△T=T-Td, while Td denotes
322 dew point temperature) was lower than 1 (Figure 3(c)), which indicating that vapor
323 pressure was saturated. An accompanying analysis using WRF/Chem of the simulated
324 cloud water mixing ratio was the highest during this period over the GZ area and
325 higher value was found around 06:00 LT (Figure 3(e-f)). This combination promoted
326 the existence of fog/low cloud.
327 Further analysis was done by looking at measurements of SO_2 (data from
328 Guangzhou Environmental Protection Bureau, http://www.gzepb.gov.cn/). The
329 diurnal variation on 8th May showed a unique pattern compared with the mean diurnal
330 pattern as measured during 2009-2011(Figure 3(d)). On this day, the SO_2
331 concentration decreased dramatically from 05:00-07:00 LT, which is consistent with
332 SO_2 transferred from gas to aqueous phase due to the high solubility of SO_2 in fog

Atmos. Chem. Phys. Discuss., doi:10.5194/acp-2016-390, 2016
Manuscript under review for journal Atmos. Chem. Phys.
Published: 13 May 2016

Atmospheric Chemistry and Physics Discussions

water droplets (Zhang et al., 2013b).

Simulation of these conditions using WRF/Chem indicates that rapid growth of both Aitken and accumulation mode sulfate started at 07:00 LT and peaked at 08:00-09:00 LT (Figure 3(g-h)). This further supports the conclusion of fresh sulfate production, in this case through both the aqueous and potential initial gas to particle formation, followed by condensation/coagulation and uptake into the liquid droplets present. All of this is consistent with generalized urban modeling studies performed under similar conditions (e.g. Cohen and Prinn (2011]).

3.4. Observed interactions between nitrate and chloride depletion

The mass size distribution of sodium and chloride showed a similar pattern to nitrate at the three sites, peaking in coarse mode particles (Figure 4) with an average percentage of 43%, 62% and 43% for coarse mode sodium, 53%, 76% and 74% for coarse mode chloride in GZ, ZH and JFM, respectively. The percentage of chloride depletion ($\%Cl_{dep}$) (Figure 5) was calculated using Eq. (2), where [Cl_{meas}^{-}] and [Na_{meas}^{+}] are the measured equivalent concentrations of chloride and sodium respectively [Yao et al., 2003b].

$$\%Cl_{dep} = \frac{1.174\left[Na^{+}_{meas}\right] - \left[Cl^{-}_{meas}\right]}{1.174\left[Na^{+}_{meas}\right]} * 100\% \quad (2)$$

In general, the $\%Cl_{dep}$ decreased as the aerosol mass increased. The relationship was strongly pronounced for fine mode sea salt particles, having a significant relationship between sodium and chloride at the three sites (R= [0.50, 0.61], P<0.05). On the other hand, there was no statistically significant correlation found in the coarse

Atmos. Chem. Phys. Discuss., doi:10.5194/acp-2016-390, 2016
Manuscript under review for journal Atmos. Chem. Phys.
Published: 13 May 2016

355 particles. Chloride had been almost entirely depleted in fine mode particles with only
356 53% and 31% depleted in fine mode particles in ZH and JFM, while there was 89%
357 and 91% depleted in coarse particles in ZH and JFM. The result is consistent with a
358 study conducted in South China Sea in 2004 as well as theory that reaction between
359 sulfuric acid and nitric acid with sea salt (sodium chloride) is facilitated in fine
360 particles due to their larger surface areas to volume ratio (Chatterjee et al., 2006; Hsu
361 et al., 2007).

362 The ratio of calculated ammonium to measured ammonium was used to explain
363 the presence of sulfuric acid and nitric acid in the aerosol, with a value larger than 1
364 indicating there was insufficient ammonium to neutralize nitric acidic NO_3^- (since
365 ammonium first consumes sulfuric acid). The calculated ratio was much higher than 1
366 in ZH and JFM suggesting that nitrate plays a role in Cl depletion. The ratio of nitrate
367 to percent chloride depletion can then be used to calculate the contribution of coarse
368 nitrate to chloride depletion (Zhuang et al., 1999; Zhao and Gao, 2008b). This result
369 showed that nitrate was responsible for the depletion of 54% and 17% of coarse
370 chloride in ZH and JFM respectively. This suggests that the interaction of sea salt
371 particles with anthropogenic pollutants is an important pathway for the generation of
372 aerosol species in coastal suburban regions like ZH, which have sizable amounts of
373 both sea salt and NO_x emissions.

374 Furthermore, we analyzed the chloride depletion rate in coastal ZH and JFM
375 under different air masses conditions, and found the total chloride depletion was 88.0%
376 and 53.5% when the air masses came from the ocean, as compared with 91.2% and

Atmos. Chem. Phys. Discuss., doi:10.5194/acp-2016-390, 2016
Manuscript under review for journal Atmos. Chem. Phys.
Published: 13 May 2016

53.8% when the air masses came from the continent. In general, the mean RH was 82.5% when the air masses came from the ocean, while the RH was 78.3% when the air masses came from the continent. The consistent finding is that there was a higher percentage of chloride depletion found when the air was relatively less humid, suggesting another important non-linear effect between maritime aerosols anthropogenic NOx (Chatterjee et al., 2010; Liu et al., 2008).

Relative humidity exceeded 80% during the whole sampling time in ZH except for 24th May, which was 64%. The percentage of chloride depletion was 95% and 69% in fine and coarse particles on 24th May, respectively. The only other day which had a significant continental wind source at ZH also had a higher relative humidity (80%), on 7th June. On that day the percentage of chloride depletion was 78% and 64% respectively. While there was no distinct difference found in coarse particles for the two cases, there was a considerable difference in the chloride depletion of the fine particles. This finding is consistent with our understanding of the release of hydrochloric acid under the known high nitric acid conditions, especially when there is less aerosol water (at lower relatively humidity) to dissolve all of the volatiles, as already discussed in the sections above (Chen et al., 2013; Dasgupta et al., 2007).

3.5. The effects of long-range transport, and in-situ chemistry

There were four days that the amounts and properties of the aerosols were significantly impacted by long range transport and unique formation and alteration

Atmos. Chem. Phys. Discuss., doi:10.5194/acp-2016-390, 2016
Manuscript under review for journal Atmos. Chem. Phys.
Published: 13 May 2016

Atmospheric Chemistry and Physics Discussions

398 mechanisms: one in each GZ and ZH (both occuring on 12th June) and three in JFM
399 (1st, 3rd, and 5th June).

400 On 12th June in both GZ and ZH, the total aerosol concentration was the highest
401 measured, at respectively 93.7 and 35.1 μg m^{-3} in GZ and ZH (Figure S1). Secondly,
402 the concentration of secondary soluble ions was the highest measured, in GZ based on
403 the Sulfur Oxidation Ratio and Nitrogen Oxidation Ratio (Sun et al., 2006), with the
404 respective values being 0.20 (SOR) and 0.17 (NOR) over the 0.44-1.0μm (Figure 6
405 (a-b)) (no supported data to estimate SOR and NOR in ZH on this day),. Thirdly, this
406 was the only day in GZ that the nitrate size distribution was found to be uni-modal,
407 where it peaked in the 1.0-1.44μm size range (Figure 6 (d)), which was the largest of
408 any mean size nitrate in GZ measured. Meanwhile, the nitrate size distribution
409 changed from coarse mode to bi-modal and peaked in 0.25-0.44 μm size range in ZH
410 measured on this day (Figure S2(j)). Fourthly, the peak of sulfate and ammonia
411 shifted from typical values in the 0.44-1.0 μm size range to the 1.0-1.44 μm size range
412 (Take GZ for example, Figure 6(c) and Figure S2(f)). All of these are consistent with
413 enhanced secondary production. Such a statistically enhanced amount of secondary
414 production requires the aerosols to have had considerably more time in the
415 atmosphere to have aged as they have, and therefore is consistent with them having
416 undergone considerable long range transport (Cohen et al., 2011).

417 To provide further evidence, 3-day air mass backward trajectories were conducted
418 at each of the three sites. The parcels were released at initial heights of 100, 500,
419 1000 and 2000m, hourly, as a means of robustly sampling the boundary layer

Atmos. Chem. Phys. Discuss., doi:10.5194/acp-2016-390, 2016
Manuscript under review for journal Atmos. Chem. Phys.
Published: 13 May 2016

Atmospheric Chemistry and Physics Discussions

throughout the day. The results showed that air masses winded up over GZ and ZH in the lower free troposphere or near the top of the boundary layer had mostly originated over continental Southeast Asia, while those winding up near the surface, had mostly come from Northern China (Take GZ for example, Figure S2(a)). Furthermore, since the air masses came from opposite directions at nearly the same time, the end result was observed to be a stable meteorological condition over GZ (very low wind 0.1 m s^{-1}) and ZH (wind speed was 1m/s which was the lowest during the sampling times). In fact, it seems from the back trajectory analysis that there was descending air in and around GZ and ZH on this day, which implies that air transported from far away in the lower free-troposphere would have been transported back near the surface (Take GZ for example, Figure S2 (b-c)). All of these results were further consistent with the high levels of aerosols measured as well as additional secondary processing having had time to occur.

FLEXPART-WRF was next applied to address the issue of the air residence time through the column over GZ and ZH on that day. Take GZ for example, as can be shown in Figure 6 (e-f), there was a strong influence from the region local to GZ and surrounding adjoining cities, at a lower altitude (500m and lower) (Figure 6(e) and Figure S2 (d-e)). Also, the results showed that air from far away was contributing mostly to the residence time at higher altitudes, yet still in the boundary layer, at 1000m and above (Figure 6(f)). This is further evidence that indeed long-range transport was also responsible.

Furthermore, the ratio of OC to EC concentrations was the minimum measured

Atmos. Chem. Phys. Discuss., doi:10.5194/acp-2016-390, 2016
Manuscript under review for journal Atmos. Chem. Phys.
Published: 13 May 2016

Atmospheric Chemistry and Physics Discussions

values on the 12th June, with a mean ratio of 1.32 and 2.39 in GZ and ZH, respectively . Also, OC showed a bi-modal distribution, although predominantly in the fine mode while EC mostly peaked at fine mode particles (Take GZ for example, Figure S2 (g-h)), indicating that the organic aerosol was mostly primary, as would be expected from large fire sources. Additionally, the potassium concentration on the 12th June was about 2-3 times higher than that of mean value measured in GZ and ZH(Take GZ for example, Figure 10(a-b)) All of these findings above, including the time of the year and the location, are consistent with the existance of biomass burning over Southeast Asia being a likely source (Cohen, 2014).

At JFM the total aerosol concentration was highest on the 1st, 3rd, and 5th June. In particular, the levels of EC and potassium were elevated on all three days, and the ratio of OC to EC was depressed (Figure S3 (c-e)). However, in addition to these clues, there were some differences: the levels of sulfate and ammonia were remarkably elevated on the 3rd and 5th June (Figure 7(g) and Figure S3 (b)), likely due to a mixing of urban sources with the fire sources. On the other hand, on the 1st June, the sulfate was lower, but the nitrate was considerably higher, peaking in the coarse mode (Figure 7 (h)), likely due to mixing of South China Sea air with the fire sources.

HYSPLIT results showed that on all three of these days, the great majority of air masses arriving at JFM originated from continental Southeast Asia (Figure S3(a). However, all of these parcels of air arrived in the upper boundary layer or the lower free troposphere. By analyzing the FLEXPART-WRF runs at higher resolution, it was demonstrated that there was a strong influence of air from ocean on 1st June (Figure 7

Atmos. Chem. Phys. Discuss., doi:10.5194/acp-2016-390, 2016
Manuscript under review for journal Atmos. Chem. Phys.
Published: 13 May 2016

(a-b)) at the lower parts of the boundary layer. This is consistent with the observed non–elevated sulfate and elevated coarse nitrate on that day. Furthermore, the FLEXPART-WRF runs at higher resolution demonstrated a considerably influence of air from Southern China (urban and semi-urban Guangdong Province, including many major shipping lanes) on the 3rd and 5th June, again in the lower parts of the boundary layer (Figure 7(c-f)). This is again consistent with the observed elevated levels of sulfate, due to the in-situ processing of urban emissions as the air was transported to JFM, and then mixing with the fire emissions transported from the other direction at height. Additionally, there was some amount of fine mode nitrate found on the 3rd Jun., further consistent with the in-situ processing of NO_2 emitted along with biomass combustion, and therefore further evidence that mixing occurred between the two different source regions.

3.6. Quantifying the impacts of fires

Taking a first look at the possibility that fires are responsible, as described above, we look at a summary of the statistics of the MODIS Fire Hotspots (Figure 8). As we observe, while the total number of fire hotspots occurring throughout Southeast Asia is moderate in early May, the number reduces to the extent that there are effectively almost no burning parcels. Furthermore, those few square kilometers that are burning are of low radiative intensity, under 200W/m^2, and hence only moderately or lowly emitting, with the exception of a single day in late June, after the period of interest has ended. This result shows that the fires themselves are not very important, or are

Atmos. Chem. Phys. Discuss., doi:10.5194/acp-2016-390, 2016
Manuscript under review for journal Atmos. Chem. Phys.
Published: 13 May 2016

Atmospheric Chemistry and Physics Discussions

mostly obscured, which is consistent with previous findings over the region of both high cloud cover and a large number of small or otherwise hard to detect fires (Cohen, 2014; Giglio, 2006).

Instead, we follow the approach of Cohen (2014) and instead look at the once to twice daily measured AOD data (Figure 9), in the context of the Empirical Orthogonal Functions approach. The rationale is that over Southeast Asia there are only a few known large urban centers (Hanoi, Ho Chi Minh City, and Bangkok). Therefore, any other significant contribution to the variance of measured AOD must be from fires. The EOF technique has been shown to be an optimal manner by which to reproduce both the spatial extent of and magnitude of the smoke over Continental Southeast Asia (Cohen, 2014; Cohen and Leocure, 2015).

As observed, the major regions of high AOD (average AOD > 0.4) are found over Southeast Asia as described above, with most of the sources coming from fires found in two arcs: one from Eastern Thailand, through Laos, and ending in Central Vietnam; and the other in the forests of Myanmar. The region around Hanoi is hard to descipher, as it could be urban expansion or fire. Additionally, there are regions found in urban East Asia, including the region between Hong Kong and Guangzhou and urbanization along the Yangtze River, however, all of these are known regions of urbanization and are not regions where fire is important (Figure 10).

An EOF Analysis concludes that in fact these are the only two statistically significant EOFs. The measured AOD over both of these regions is clearly elevated compared with the region as a whole throughout the entire time. Furthermore, there is

Atmos. Chem. Phys. Discuss., doi:10.5194/acp-2016-390, 2016
Manuscript under review for journal Atmos. Chem. Phys.
Published: 13 May 2016

Atmospheric Chemistry and Physics Discussions

an especially large contribution from these two EOFs compared with the background over Southeast Asia only (excluding AOD measured over China, which is downwind and hence not a fire source region) from May 31st to June 6th. Given the rapid transport time from Southeast Asia to JFM, the fact that these peaks occur within 1 day of the peaks in the fires is reasonable. Additionally, while the overall Southeast Asian AOD drops from the 8th onwards, there is a very significant difference (difference in AOD more than 0.5) between the overall AOD and that over the two source regions again from June 8th to June 13th. Given that there are markers of fires in GZ and ZH on June 12th, including high potassium and a low OC/EC ratio, and that a significant portion of the airflow over these regions originated from Southeast asia within the past 72 hours, these results are consistent with high fires originating from Southeast Asia then being transported over the next 72 hours to GZ and ZH. The fact that only one day has such measured conditions at the surface is likely due to the fact that the smoke is mostly concentrated near the boundary layer and hence local vertical mixing was most prevelant on or around June 12th.

4. Conclusion

Aerosol samples were collected at three sites using a 6-stage sampler during the local wet season in Southern China (May – Jun.) in 2010, to jointly study the mass and size distributions of aerosol chemical components. Based on specific case studies, some models of the air flow, and remote sensing, the impacts of chemistry and atmospheric transport were investigated on the aerosol formation mechanisms at the

Atmos. Chem. Phys. Discuss., doi:10.5194/acp-2016-390, 2016
Manuscript under review for journal Atmos. Chem. Phys.
Published: 13 May 2016

three sites over Southern China. These were chosen such that they spanned different source and meteorological regions, at urban site GZ, a suburban site ZH, and a remote and forested site at JFM.

Sulfate and Ammonium were found to have a singly peaked distribution from 0.44-1.0μm at all sites over the entire sampling period in this study, and accounted for 57.5-99 % of the daily-average total aerosol mass. Aqueous-phase reactions were found to be an essential factor to the formation of droplet sulfate. In addition, we found significant secondary processing and enhancement due to meteorological drivers which were wetter or allowed for a longer residence time.

A bi-modal distribution was found for nitrate, with a droplet mode in 0.44-1.0μm, indicating that it was formed under heavily polluted conditions or through similar secondary aerosol processing. On the other hand, nitrate had a significant fraction in the coarse mode in ZH and JFM during the wet season, where it accounted for about 40% of total mass. In this case, we found that the mass size distribution of nitrate was likely attributed with chloride depletion, with almost complete chloride depletion found in ZH and JFM during the wet season. Additionally, relative humidity was an important consideration in chloride depletion under relatively lower relative humidity, conditions, further leading to the increase of coarse mode nitrate.

OC and EC showed a broad peak at 0.25-1.0μm in GZ and ZH, consistent with significant local sources, from urbanization, transport, residential, and shipping sources. Furthermore, under less heavily polluted conditions, OC was found to have a bi-modal distribution in JFM, with important contributions from secondary particle

Atmos. Chem. Phys. Discuss., doi:10.5194/acp-2016-390, 2016
Manuscript under review for journal Atmos. Chem. Phys.
Published: 13 May 2016

552 formation in the fine mode and potential biological aerosol in the coarse mode
553 particles.
554 Additionally, they were shown to have broad peaks, and a significantly different
555 ratio, raising the likelihood of a mixing of the local emissions with emissions
556 transported long-range from biomass burning in Southeast Asia. These conditions
557 were further supported by large amount of potassium found jointly with the aerosol.
558 An in-depth analysis of the meteorology, and remotely sensed Fire and AOD
559 properties, in conjunction with a variance maximizing technique, provided further
560 evidence to help us validate this assumption. It is clear that there was a significant
561 impact on GZ and ZH from fires sources from Thailand, Laos, and Vietnam, as well
562 as possible long-range transport of urban emissions from the urban megacity of Hanoi
563 in Vietnam. The combination of local formation and long-range transport played a
564 significant role on the variation of particles chemical compositions.
565 Overall, we found that the size distribution and formation of aerosols greatly
566 depend on emissions, location, and in-situ processing, especially aqueous-phase
567 reactions. Strong local formation and long-range-transport of both urban pollution
568 from GZ and of biomass burning from Southeast Asia all were observed to influence
569 the size distribution of chemical components across all of the areas studies. On the
570 other hand, the interaction between sea salt aerosols and anthropogenic pollutants
571 showed significant effects at coastal locations and play an important role in the
572 deterioration of the air quality in Southern China under high relative humidity
573 conditions during the wet season.

574

575 **Acknowledgments**

576 This work was supported by National Science Fund for Outstanding Young Scholars
577 (41425020), China Special Fund for Meteorological Research in the Public Interest
578 (GYHY201406031), National Science & Technology Pillar Program
579 (2014BAC21B02) and Specialized Research Fund for the Doctoral Program of
580 Higher Education in China (2013380004115009). The authors would especially like
581 to thank Prof. Guenter Engling at National Tsing Hua University for helping to
582 chemical analysis at the laboratory.

583

584 **References**

585 Anlauf, K., Li, S.M., Leaitch, R., Brook, J., Hayden, K., Toom-Sauntry D., and Wiebe,
586 A.: Ionic composition and size characteristics of particles in the Lower Fraser
587 Valley: Pacific 2001 field study, Atmospheric Environment, 40, 2662- 2675, doi:
588 10.1016 /j.atmosenv. 2005.12.027, 2006.
589 Barth, M.C., Hegg, D.A., and Hobbs, P.V.: Numerical modeling of cloud and
590 precipitation chemistry associated with two rainbands and some comparisons with
591 observations, Journal of Geophysical Research, 97, 5825- 5845, doi:
592 10.1029/92JD00464, 1992.
593 Brioude, J., Arnold, D., Stohl, A., Gassiani, M., Morton, D., Seibert, P., Angevine, W.,
594 Evan, S., Dingwell, A., Fast, J.D., Easter, R.C., Pisso, I., Burkhart, J., and
595 Wotawo, G.: The Lagrangian particle disperation model FLEXPART-WRF

version 3.1, Geoscientific Model Development, 6, 1889-1904, doi: 10.5194/gmd-6-1889-2013, 2013.

Burnett, R.T., et al.: An integrated risk function for estimating the global burden of disease attributable to ambient fine particulate matter exposure, Environmental Health Perspectives, 122, 397, doi:10.1289/ehp.1307049,2014.

Cao, J.J., Lee, S.C., Ho, K.F., Zou, S.C., Fung, K., Li, Y., Watson, J.G., and Chow, J. C.: Spatial and seasonal variations of atmospheric organic carbon and elemental carbon in Pearl River Delta Region, China, Atmospheric Environment, 38, 4447–4456, doi:10.1016/j.atmosenv.2004.05.016, 2004.

Chatterjee, A., Dutta, C., Sen, S., Ghosh, K., Biswas, N., Ganguly, D., and Jana, T.K.: Formation, transformation, and removal of aerosol over a tropical mangrove forest, Journal of Geophysical Research, 111, D24302, doi:10.1029/2006JD007144, 2006.

Chatterjee, A., Adak, A., Singh, A.K., Srivastava, M.K., Ghosh, S.K., Tiwari, S., Devara, P.C.S., and Raha, S.: Aerosol chemistry over a high altitude station at northeastern Himalayas, India, PLoS ONE, 5, e11122, doi: 10.1371/journal.pone.0011122, 2010.

Chen, H.Z., Wu, D., Liao, B.T., Mao, X., Zhuang, H.B., Li, L., Liu, A.M., Li, H.Y., and Li, F.: Influence of different acidic gases and relative humidity on the chlorine loss of marine aerosols, Acta Scientiae Circustantiae, 33, 1141-1149, 2013(in Chinese with English abstract).

Clegg, S.L., Brimblecombe, P., and Wexler, A.S.: Thermodynamic Model of the

System H^+–NH_4^+–SO_4^{2-}–NO_3^-–H_2O at Tropospheric Temperatures, The Journal of Physical Chemistry A, 102, 2137-2154, doi: 10.1021/jp973042r, 1998.

Cohen, J. B.: Quantifying the Occurrence and Magnitude of the Southeast Asian Fire Climatology, Environmental Research Letter, 9, 114018, doi:10.1088/1748-9326/9/11/114018, 2014.

Cohen, J. B., and Prinn, R.G.: Development of a fast, urban chemistry metamodel for inclusion in global models, Atmospheric Chemistry and Physics, 11, 7629-7656, doi:10.5194/acp-11-7629-2011, 2011.

Cohen, J. B., and Wang, C.: An Estimate of Global Black Carbon Emissions Using a Top-Down Kalman Filter Approach, Journal of Geophysical Research , 119, 1-17, doi:10.1002/2013JD019912, 2013.

Cohen J.B., and Lecoeur, E.: Decadal-scale relationship between measurements of aerosols, land-use change, and fire over Southeast Asia, Atmospheric Chemistry and Physics, 15, 26895-26957, 2015.

Cohen, J. B., Prinn, R.G., and Wang, C.: The Impact of detailed urban-scale processing on the composition, distribution, and radiative forcing of anthropogenic aerosols, Geophysical Research Letters, 38, L10808, doi:10.1029/2011GL047417, 2011.

Chung S.H., and Seinfeld, J.H.: Climate response of direct radiative forcing of anthropogenic black carbon, Journal of Geophysical Research, 110, D11102, doi: 10.1029/2004JD005441, 2005.

Dasgupta, P.K., Campbell, S.W., Al-Horr, R.S., Ullah, S.M.R., Li, J.Z., Amalfitano, C.,

and Poor, N.D.: Conversion of sea salt aerosol to $NaNO_3$ and the production of HCl: Analysis of temporal behavior of aerosol chloride/nitrate and gaseous HCl/HNO_3concentrations with AIM, Atmospheric Environment, 41, 4242-4257, doi:10.1016/j.atmosenv.2006.09.054, 2007.

Delene, D.J. and Ogren, J.A.: Variability of aerosol optical properties at four North American surface monitoring sites, Journal of the Atmospheric Sciences, 59, 1135-1150, doi: http://dx.doi.org/10.1175/ 1520-0469(2002)059 <1135:VOAOPA> 2.0.CO;2, 2002.

Draxler, R.R., and Hess, G.D.: An overview of the HYSPLIT_4 modeling system of trajectories, dispersion, and deposition, Australian Meteorological Magazine, 47, 295-308, 1998.

Dubovik, O., Smirnov, A., Holben, B.N., King, M.D., Kaufman, Y.J., Eck, T.F., and Slutsker, I.: Accuracy assessments of aerosol optical properties retrieved from Aerosol Robotic Network (AERONET) Sun and sky radiance measurements, Journal of Geophysical Research, 105, 9791-9806, doi: 10.1029/2000JD900040, 2000.

Ervens, B., Turpin, B.J., and Weber, R.J.: Secondary organic aerosol formation in cloud droplets and aqueous particles (aqSOA): a review of laboratory, field and model studies, Atmospheric Chemistry and Physics, 11, 11069-11102, doi:10.5194/acp-11-11069-2011, 2011.

Giglio, L., Kendall, J.D., and Mack, R.: A multi-year active fire data set for the tropics derived from the TRMM VIRS, International Journal of Remote Sensing, 24,

4505- 4525, doi: 10.1080/0143116031000070283, 2003.

Giglio, L., Csiszar, I., and Justice, C.O.: Global distribution and seasonality of active fires as observed with the Terra and Aqua Moderate Resolution Imaging Spectroradiometer (MODIS) sensors, Journal of Geophysical Research, 111, G02016, doi: 10.1029 / 2005JG000142, 2006.

Han, Y., Han, Z., Cao, J.J., Chow, J.C., Watson, J.G., An, Z.S., Liu, S.X., and Zhang, R.J.: Distribution and origin of carbonaceous aerosol over a rural high-mountain lake area, Northern China and its transport significance, Atmospheric Environment, 42, 2405-2414, doi:10.1016/j.atmosenv.2007.12.020, 2008.

Harrison, R.M., and Pio, C.A.: Size differentiated composition of inorganic atmospheric aerosols of both marine and polluted continental origin, Atmospheric Environment, 17, 1733-1738, doi:10.1016/0004-6981(83)90180-4, 1983.

Huang, X.F., Yu, J.Z., He, L.Y., and Hu. M.,: Size distribution characteristics of elemental carbon emitted from Chinese vehicles: results of a tunnel study and atmospheric implications, Environmental Science & Technology, 44, 5355–5360, doi: 10. 1021 /es0607281,2006.

Hsu, S.C., Liu, S.C., Kao, S.J., Jeng, W.L., Huang, Y.T., Tseng, C.M., Tsai, F.J., Tu, J.Y., and Yang, Y.: Water-soluble species in the marine aerosol from the northern South China Sea: High chloride depletion related to air pollution, Journal of Geophysical Research, 112, D19304, doi:10.1029/2007JD008844,2007.

Kim, S.W., Berthier, S., Raut, J.C., Chazette, P., Dulac, F., and Yoon, S.C.: Validation of aerosol and cloud layer structures from the space-borne lidar CALIOP using a

684 ground-based lidar in Seoul, Korea, Atmospheric Chemistry and Physics, 8,
685 3705-3720, doi:10.5194/acp-8-3705-2008, 2008.
686 Jacobson, M.Z.: Global direct radiative forcing due to multicomponent
687 anthropogenic and natural aerosols, Journal of Geophysical Research, 106,
688 1551-156, doi: 10.1029/2000JD900514, 2001.
689 Lan, Z.J., Chen, D.L., Li, X., Huang, X.F., He, L.Y., Deng, Y.G., Feng, N., and Hu, M.:
690 Modal characteristics of carbonaceous aerosol size distribution in an urban
691 atmosphere of South China, Atmospheric Research, 100, 51-60,
692 doi:10.1016/j.atmosres.2010.12.022, 2011.
693 Liu, S., Hu, M., Slanina, S., He, L.Y., Niu, Y.W., Bruegemann, E., Gnauk, T., and
694 Herrmann, H.: Size distribution and source analysis of ionic compositions of
695 aerosols in polluted periods at Xinken in Pearl River Delta (PRD) of China,
696 Atmospheric Environment, 42, 6284- 6295, doi:10.1016/j.atmosenv.2007.12.
697 035 ,2008.
698 Lim, Y.B., Tan, Y., Perri, M.J., Seitzinger, S.P., and Turpin, B.J.: Aqueous chemistry
699 and its role in secondary organic aerosol (SOA) formation, Atmospheric
700 Chemistry and Physics, 10, 10521-10539, doi: 10.5194/acp-10-10521-2010, 2010.
701 Meng, Z., and Seinfeld, J.H.: On the source of the submicrometer droplet mode of
702 urban and regional aerosols, Aerosol Science and Technology, 20, 253- 265, doi:
703 10.1080 /02786829408959681, 1994.
704 Myhre, G., et al.: Radiative forcing of the direct aerosol effect from AeroCom Phase
705 II simulations, Atmospheric Chemistry and Physics, 13, 1853-1877,

706 doi:10.5194/acp-13-1853-2013, 2013.

707 Petrenko, M., Kahn, R., Chin, M., Soja, A., Kucsera, T., and Harshvardhan,: The use
708 of satellite-measured aerosol optical depth to constrain biomass burning emissions
709 source strength in the global model GOCART, Journal of Geophysical Research,
710 117, D18212, doi: 10.1029/2012JD017870, 2012.

711 Pierson, W.R., and Brachaczek, W.W.: Coarse and fine particle atmospheric nitrate
712 and HNO_3(g) in Claremont, California, during the 1985 nitrogen species methods
713 comparison study, Atmospheric Environment, 22, 1665–1668, doi:10.1016/
714 0004-6981(88)90394-0, 1998.

715 Pillai, P.S., and Moorthy, K.K.: Aerosol mass-size distributions at a tropical suburban
716 environment: response to mesoscale and synoptic processes, Atmospheric
717 Environment, 35, 4099- 4112, doi:10.1016/S1352-2310(01)00211-4, 2001.

718 Pio, C., Legrand, M., Oliveira, T., Afonso, J., Santos, C., Caseiro, A., Fialho, P.,
719 Barata, F., Puxbaum, H., Sanchez-Ochoa, A., Kasper-Giebl, A., Gelencsér, A.,
720 Preunkert, S., and Schock, M.: Climatology of aerosol composition (organic
721 versus inorganic) at nonurban sites on a west–east transect across Europe, Journal
722 of Geophysical Research-Atmospheres, 112, D23S02, 10.1029/2006JD008038,
723 2007.

724 Ramanathan, V., and Garmichael, G.: Global and regional climate changes due to
725 black carbon, Nature Geoscience, 1, 221-227, doi:10.1038/ngeo156, 2008.

726 Remer, L.A., Mattoo, S., Levy, R.C., Munchak, L.A.: MODIS 3km aerosol product:
727 algorithm and global perspective, Atmospheric Measurement Techniques, 6,

728 1829–1844, doi:10.5194/amt-6-1829-2013, 2013.

729 Rosenfeld, D., Sherwood, S., Wood, R., and Donner, L.: Climate effects of aerosol-
730 cloud interactions, Science, 343, 379-380, doi: 10.1126/science.1247490, 2014.

731 Schuster, G.L., Dubovik, O., and Holben, B.N.: Angstrom exponent and bimodal
732 aerosol size distributions, Journal of Geophysical Research, 111, D07207, doi: 10.
733 1029 /2005JD006328,2006.

734 Seinfeld, J., and Pandis, S.: Atmospheric Chemistry and Physics: From Air Pollution
735 to Climate Change, John Wiley & Sons, New York, 2006.

736 Situ, S.P, Guenther, A., Wang, X.M., Jiang, X.X., Turnipseed, A., Wu, Z.Y., Bai, J.H.,
737 and Wang, X.X.: Impacts of seasonal and regional variability in biogenic VOC
738 emissions on surface ozone in the Pearl River delta region, China, Atmospheric
739 Chemistry and Physics, 13, 11803- 11817, doi:10.5194/acp-13-11803-2013, 2013.

740 Stohl, A., Hittenberer, M., and Wotawa, G.: Validation of the Lagrangian particle
741 dispersion model Flexpart against large-scale tracer experiment data, Atmospheric
742 Environment, 32, 4245-4264, doi:10.1016/S1352-2310(98)00184-8, 1998.

743 Sun, Y.L., Zhuang, G.S., Tang, A.H., Wang, Y., and An, Z.S.: Chemical characteristics
744 of $PM_{2.5}$ and PM_{10} in haze-fog episodes in Beijing, Environmental Science and
745 Technology, 40, 3148- 3155, doi: 10.1021/es051533g, 2006.

746 Tao, J., Ho, K.F., Chen, L.G., Zhu, L.H., Han, J.L., and Xu, Z.C.: Effect of chemical
747 composition of $PM_{2.5}$ on visibility in Guangzhou, China,2007 Spring, Particulogy,
748 7, 68-75, doi: 10.1016/j.partic.2008.11.002, 2009.

749 Tsigaridis, K., et al.: The AeroCom evaluation and intercomparison of organic aerosol

750 in global models, Atmospheric Chemistry and Physics, 14, 10845-10895,
751 doi:10.5194/acp-14-10845-2014, 2014.
752 Volkamer, R., Ziemann, P.J., and Molina, M.J.: Secondary Organic Aerosol Formation
753 from Acetylene (C_2H_2): seedeffect on SOA yields due to organic photochemistry
754 in the aerosol aqueous phase, Atmospheric Chemistry and Physics, 9, 1907-1928,
755 doi: 10.5194/acp-9-1907-2009, 2009.
756 Wang, X.F., Wang, W.X., Yang, L.X., Gao, X.M., Nie, W., Yu, Y.C., Xu, P.J., Zhou, Y.,
757 and Wang, Z.: The secondary formation of inorganic aerosols in the droplet mode
758 through heterogeneous aqueous reactions under haze conditions, Atmospheric
759 Environment, 63, 68-76, doi: 10.1016/j.atmosenv.2012.09.029, 2012.
760 Wang, Z., et al.: Source and variation of carbonaceous aerosols at Mount Tai, North
761 China: results from a semi-continuous instrument, Atmospheric Environment, 45,
762 1655-1667, doi: 10.1016/j.atmosenv.2011.01.006, 2011.
763 Yao, X.H., Lau, A.P.S., Fang, M., Chan, C.K., and Hu, M.: Size distributions and
764 formation of ionic species in atmospheric particulate pollutants in Beijing, China:
765 2—dicarboxylic acids, Atmospheric Environment, 37, 3001-3007, doi:10.1016/
766 S1352-2310(03)00256-5, 2003a.
767 Yao, X.H., Fang, M. and Chan, C.K. The size dependence of chloride depletion in fine
768 and coarse sea-salt particles, Atmospheric Environment, 37, 742-751,
769 doi:10.1016/S1352-2310(02)00955-X, 2003b.
770 Zhang, Z.S., Engling, G., Chan, C.Y., Yang, Y.H., Lin, M., Shi, S., He, J., Li, Y.D.,
771 Wang, X.M.: Determination of isoprene-derived secondary organic aerosol tracers

(2-methyltetrols) by HPAEC-PAD: Results from size-resolved aerosols in a tropical rainforest, Atmospheric Environment, 70, 468- 476, doi:10.1016/j.atmosenv. 2013.01.020, 2013a.

Zhang, Q., Tie, X.X., Lin, W.L., Cao, J.J., Quan, J.N., Ran, L., and Xu, W.Y.: Variability of SO_2 in an intensive fog in North China Plain: Evidence of high solubility SO_2, Particuology, 11, 41-47, doi:10.1016/j.partic.2012.09.005, 2013b.

Zhao, Y.L., and Gao, Y.: Mass size distributions of water-soluble inorganic and organic ions in size-segregated aerosols over metropolitan Newark in the US east coast, Atmospheric Environment, 42, 4063-4078, doi:10.1016/j.atmosenv.2008.01.032, 2008a.

Zhao Y.L., and Gao, Y.: Acidic species and chloride depletion in coarse aerosol particles in the US east coast, Science of The Total Environment, 407, 541- 547, doi:10.1016/j.scitotenv.2008.09.002, 2008b.

Zhou, Y., Xue, L.K., Wang, T., Gao, X.M., Wang, Z., Wang, X.F., Zhang, J.M., Zhang, Q.Z., and Wang, W.X.: Characterization of aerosol acidity at a high mountain site in central eastern China, Atmospheric Environment, 51, 11-20, doi:10.1016/j.atmosenv.2012.01.061, 2012.

Zhuang, H., Chan, C.K., Fang, M., Wexler, A.S.: Size distributions of particulate sulfate, nitrate and ammonium at a suburban site in Hong Kong, Atmospheric Environment,33, 843- 853, doi:10.1016/S1352-2310(98)00305-7, 1999.

Atmos. Chem. Phys. Discuss., doi:10.5194/acp-2016-390, 2016
Manuscript under review for journal Atmos. Chem. Phys.
Published: 13 May 2016

Atmospheric Chemistry and Physics Discussions

792 **Figures**

793 **Figure 1.** Location of sampling sites in Southern China: GZ (Guangzhou), ZH
794 (Zhuhai), and JFM (Jianfeng Mountain).

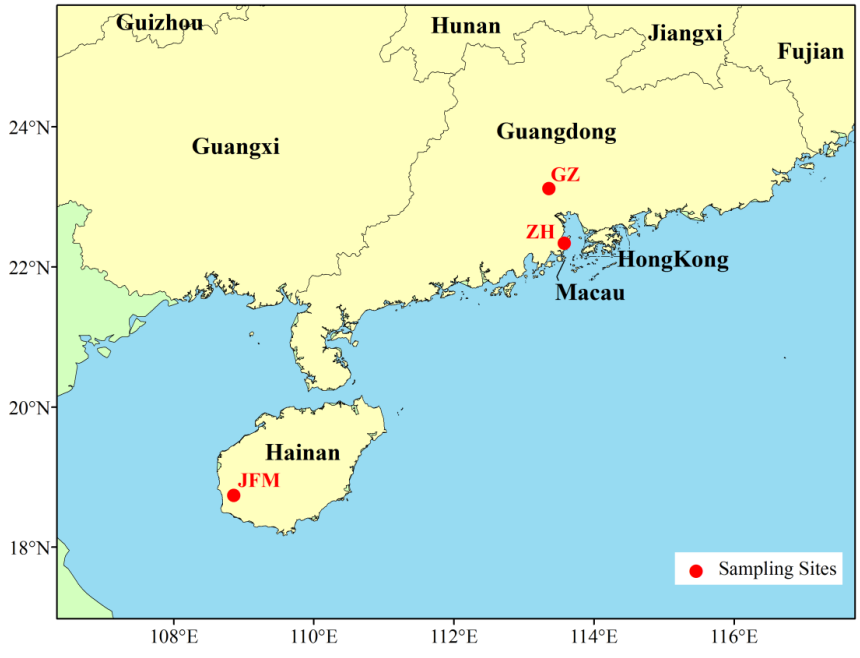

795
796

Atmos. Chem. Phys. Discuss., doi:10.5194/acp-2016-390, 2016
Manuscript under review for journal Atmos. Chem. Phys.
Published: 13 May 2016

Atmospheric Chemistry and Physics Discussions

797 **Figure 2.** The mass size distribution of major compositions (SO_4^{2-}, NO_3^-, NH_4^+, OC
798 and EC) at the three sites during study period

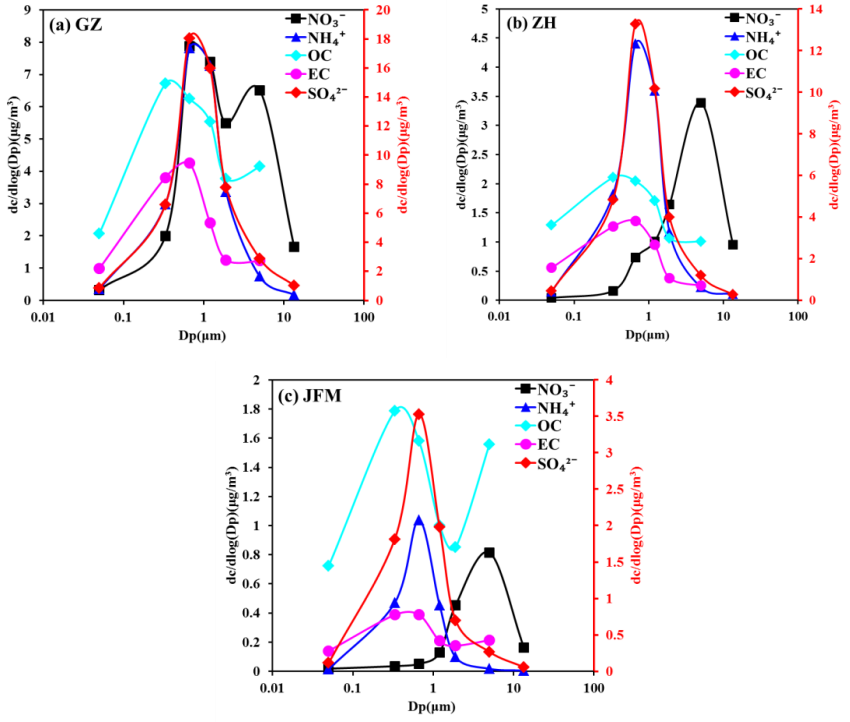

799

Atmos. Chem. Phys. Discuss., doi:10.5194/acp-2016-390, 2016
Manuscript under review for journal Atmos. Chem. Phys.
Published: 13 May 2016

Atmospheric Chemistry and Physics Discussions

800 **Figure 3.** Case study on 8th May. in GZ ((a)The cloud fraction over Southern China;
801 (b)Distribution of simulated average 2 m relative humidity at 05:00-07:00 LT; (c) The
802 time series of observational visibility, wind speed, relative humidity and the
803 depression of dew point (time resolution was 30mins); (d) The time series of
804 monitoredmean SO_2 during 2009-2010 and SO_2 on 8th May ;(e) Distribution of
805 simulated average cloud; (f) The time-height distribution of simulated cloud water
806 mixing ratio on 8th May; (g-h) The time-height of simulated Aitken and accumulation
807 mode SO_4^{2-})

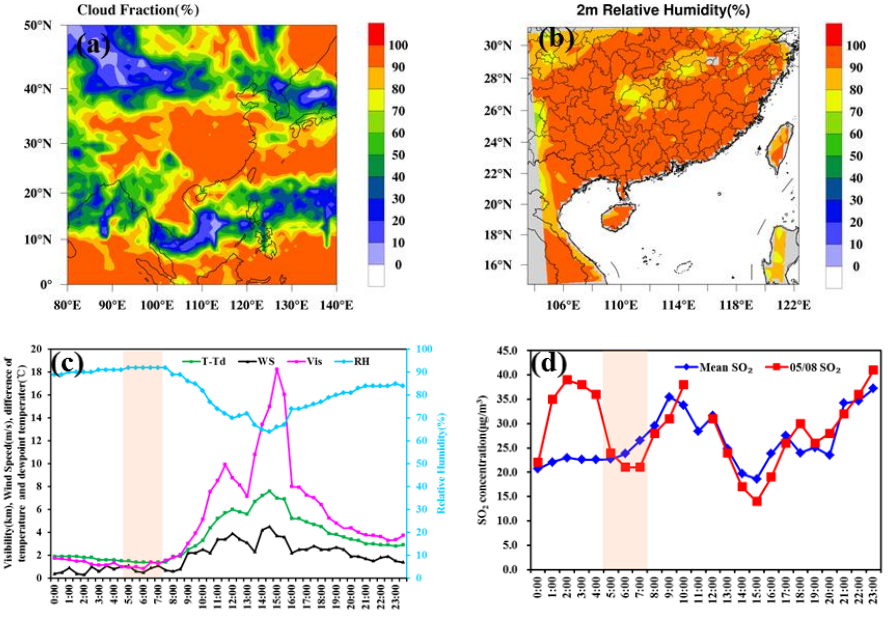

Atmos. Chem. Phys. Discuss., doi:10.5194/acp-2016-390, 2016
Manuscript under review for journal Atmos. Chem. Phys.
Published: 13 May 2016

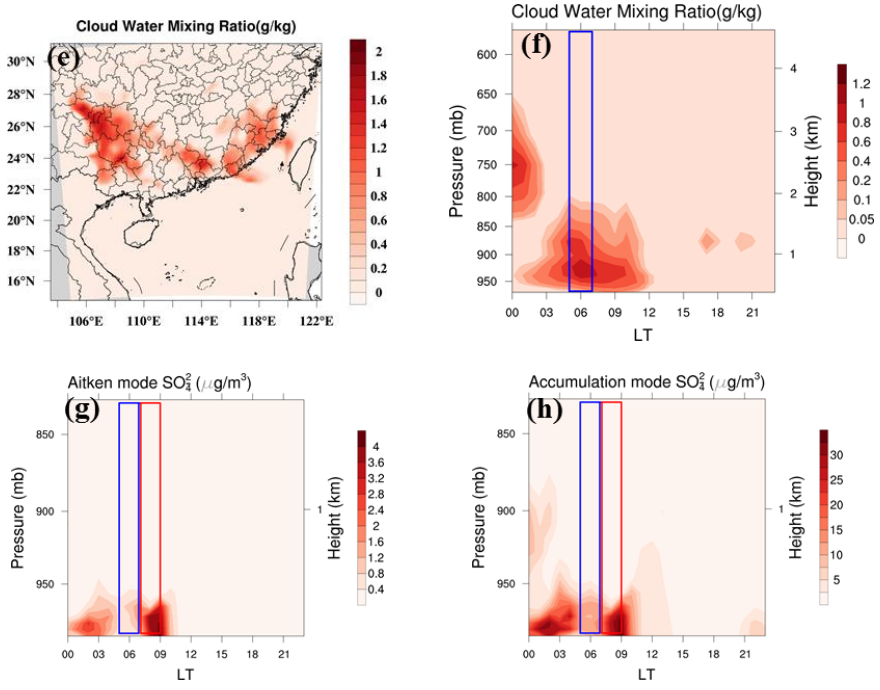

808

Atmos. Chem. Phys. Discuss., doi:10.5194/acp-2016-390, 2016
Manuscript under review for journal Atmos. Chem. Phys.
Published: 13 May 2016

Atmospheric Chemistry and Physics Discussions

809 **Figure 4.** The mass size distribution of Na^+ and Cl^- at the three sites

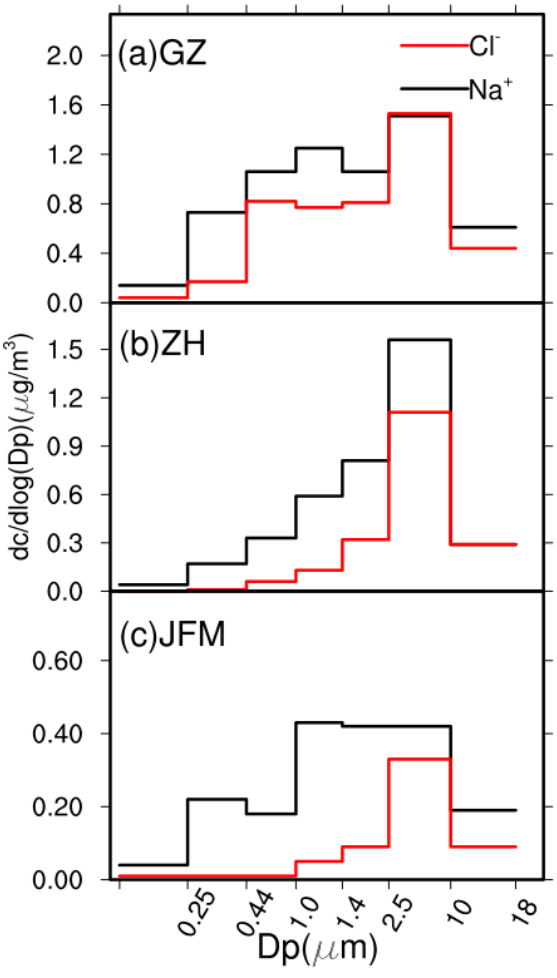

810
811

Atmos. Chem. Phys. Discuss., doi:10.5194/acp-2016-390, 2016
Manuscript under review for journal Atmos. Chem. Phys.
Published: 13 May 2016

Atmospheric Chemistry and Physics Discussions

812 **Figure 5.** The mass size distribution of percentage of chloride depletion at the three
813 sites

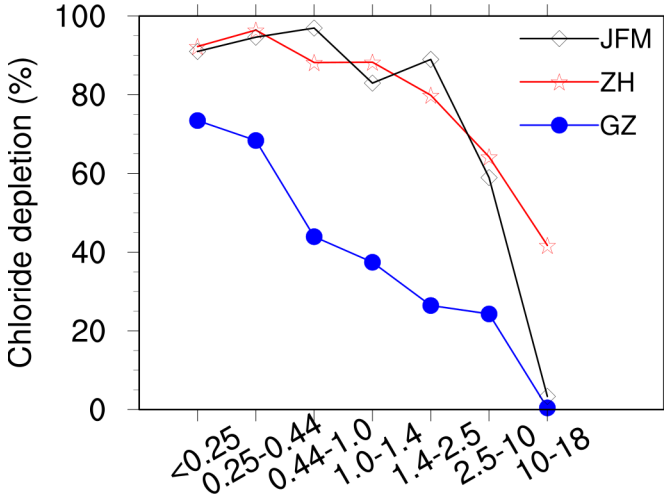

814

815

Atmos. Chem. Phys. Discuss., doi:10.5194/acp-2016-390, 2016
Manuscript under review for journal Atmos. Chem. Phys.
Published: 13 May 2016

Atmospheric Chemistry and Physics Discussions

816 **Figure 6.** Case study on 12th Jun. in GZ ((a-b) The time series of SOR and NOR; (c-d)

817 The mass size distribution of SO_4^{2-} and NO_3^-; (e-f) FLEXPART-WRF total column

818 residence times over the last 72h arriving in GZ on 12th Jun. at 100m and 1000m)

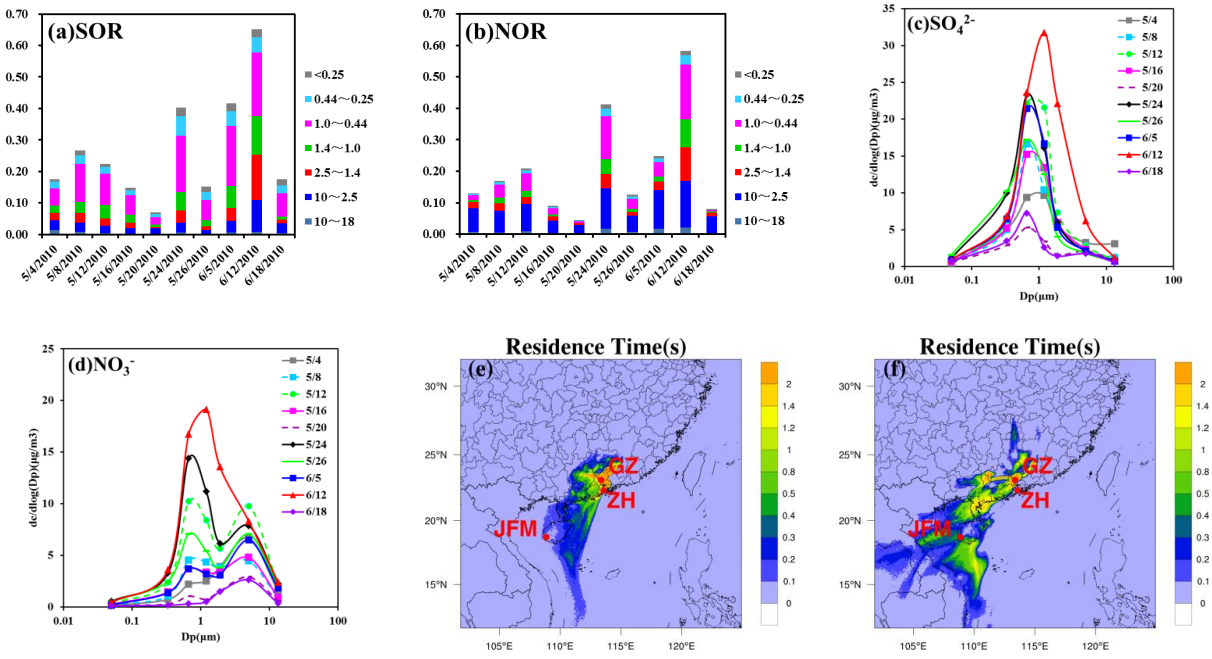

819

Atmos. Chem. Phys. Discuss., doi:10.5194/acp-2016-390, 2016
Manuscript under review for journal Atmos. Chem. Phys.
Published: 13 May 2016

Atmospheric Chemistry and Physics Discussions

820 **Figure 7.** Case study on 1st, 3rd and 5th Jun. in JFM ((a-b) FLEXPART-WRF total
821 column residence times on over the last 72h arriving in JFM on 1st Jun. at 100m and
822 1000m; (c-d) and (e-f) same at (a-b) but on 3rd and 5thJun. respectively; (g-h) The
823 mass size distribution of SO_4^{2-} and NO_3^-)

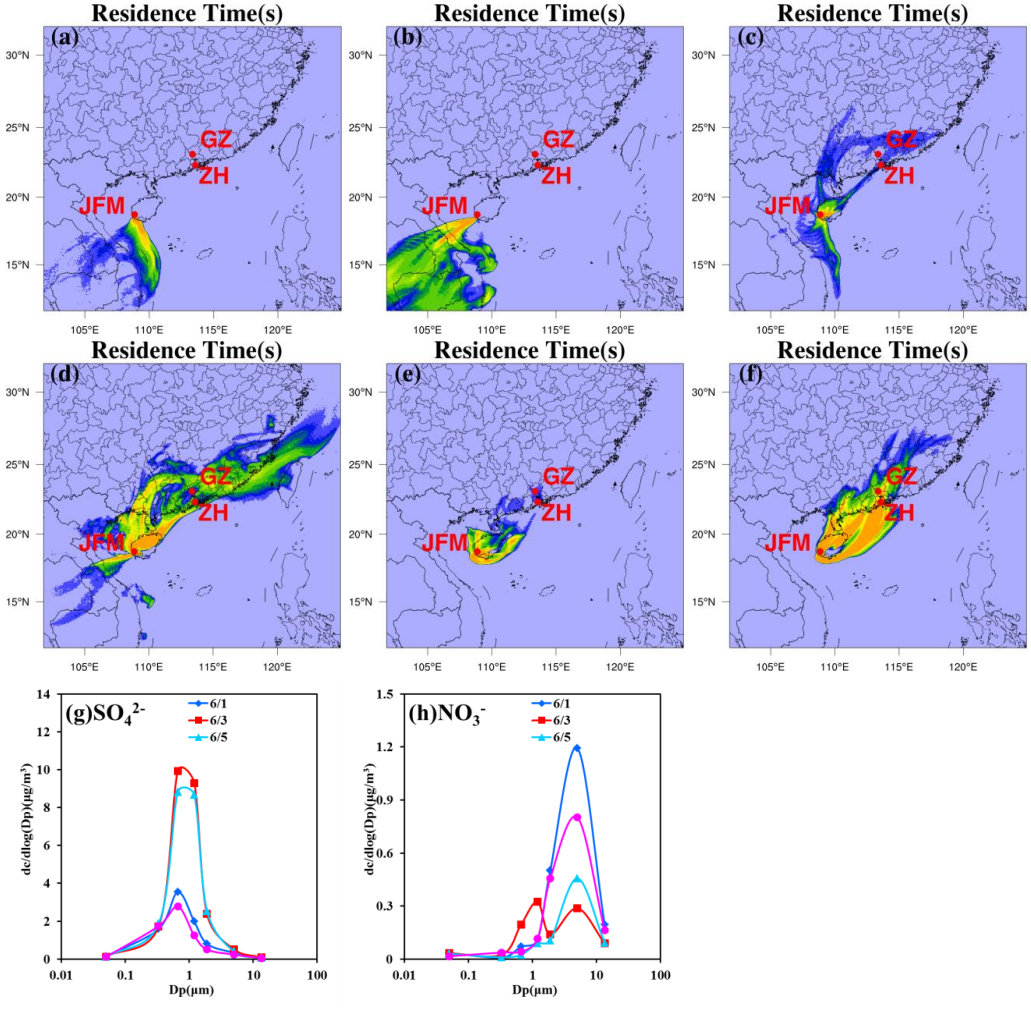

824

825

826

Atmos. Chem. Phys. Discuss., doi:10.5194/acp-2016-390, 2016
Manuscript under review for journal Atmos. Chem. Phys.
Published: 13 May 2016

Atmospheric Chemistry and Physics Discussions

827 **Figure 8.** Spatially averaged/aggregated statistics of (a) MODIS Fire numbers (Count)
828 and (b) Fire Radiative Power (FRP) over Southeast Asia for May and June 2010. The
829 statistics represent the respective Count [total number of burning 1kmx1km pixels]
830 and average FRP [W/m^2 per 1kmx1km pixel] over the whole of Southeast Asia and
831 the specific regions where the AOD (as an indicator for smoke) has its highest levels
832 of variability: EOF1 and EOF2.

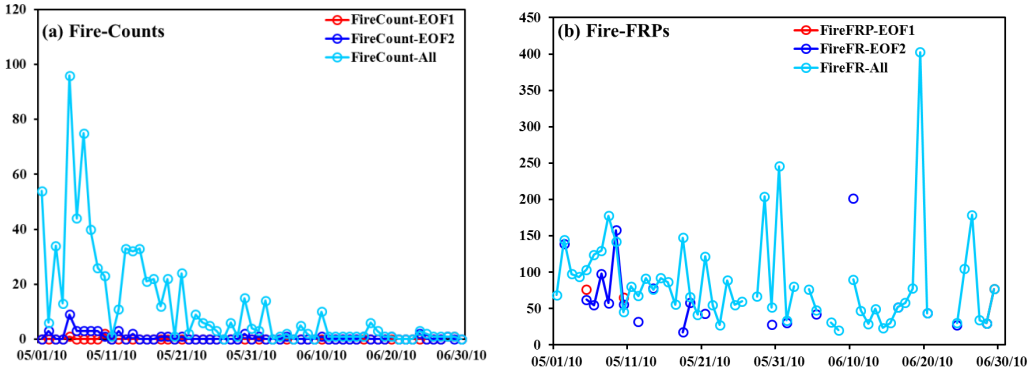

833

Atmos. Chem. Phys. Discuss., doi:10.5194/acp-2016-390, 2016
Manuscript under review for journal Atmos. Chem. Phys.
Published: 13 May 2016

Atmospheric Chemistry and Physics Discussions

834 **Figure 9.** Average spatial distribution of the (a) mean and (b) standard deviation of

835 daily MODIS AOD from May 1st through June 30th 2010

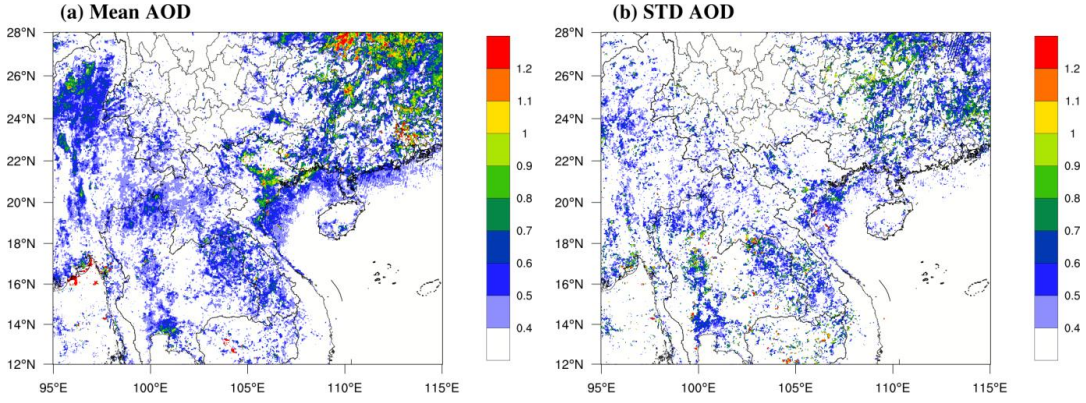

836
837
838
839
840
841
842
843
844
845
846
847
848

Atmos. Chem. Phys. Discuss., doi:10.5194/acp-2016-390, 2016
Manuscript under review for journal Atmos. Chem. Phys.
Published: 13 May 2016

Atmospheric Chemistry and Physics Discussions

849 **Figure10**. The time-varying statistics of the AOD averaged over the first two EOFs of
850 the AOD (reflecting the regions most impacted by AOD variance or smoke from fires)
851 and the average K^+ concentration and average ratio of OC/EC in the three sites.

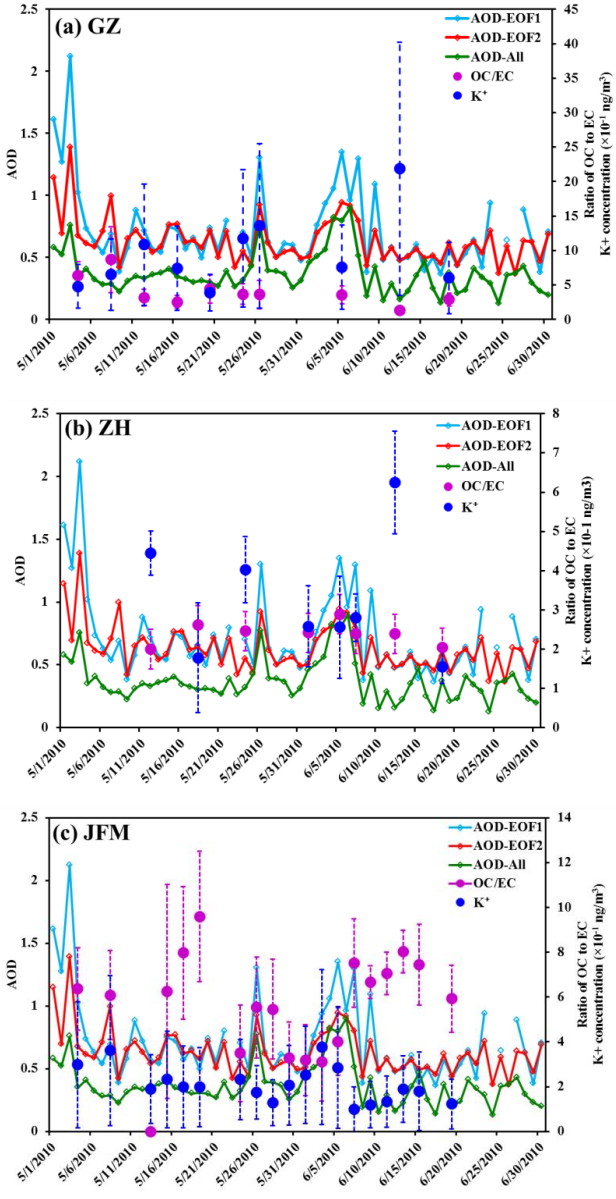

852

Atmos. Chem. Phys. Discuss., doi:10.5194/acp-2016-390, 2016
Manuscript under review for journal Atmos. Chem. Phys.
Published: 13 May 2016

Atmospheric Chemistry and Physics Discussions

853 **Tables**

854 **Table 1.** Average concentration and standard deviation [μg m^{-3}] of chemical

855 components in the given size-resolved particles (and their percentage of PM_{10}) at the

856 three sites during the 2010 wet season.

Site	Size	Sum of measured species	SO_4^{2-}	NO_3^-	NH_4^+	OC	EC
GZ	$PM_{1.0}$	24.4±10.9	8.0±3.1 (60.2)	3.0±2.4 (34.5)	3.4±1.7 (64.2)	5.5±2.0 (57.9)	2.9±2.6 (72.5)
	$PM_{2.5}$	34.9±17.3	11.7±5.2 (88.0)	5.0±4.0 (57.5)	4.9±2.9 (92.5)	7.2±2.7 (75.8)	3.4±3.2 (85.0)
	PM_{10}	46.7±20.6	13.3±5.8	8.7±5.2	5.3±3.1	9.5±3.7	4±3.8
ZH	$PM_{1.0}$	12.9±4.5	6.3±2.1 (66.3)	0.3±0. 3(10.3)	2.2±0.8 (71.0)	2.4±1.1 (66.7)	1.3±0.8 (76.5)
	$PM_{2.5}$	18.1±6.8	8.8±3.2 (92.6)	0.9±0.8 (31.0)	3.0±1.2 (96.8)	3.0±1.5 (83.3)	1.5±0.9 (88.2)
	PM_{10}	23.7±7.3	9.5±3.4	2.9±1.1	3.1±1.3	3.6±1.9	1.7±1.0
JFM	$PM_{1.0}$	4.4±1.6	1.8±1.0 (75.0)	0.1±0.1 (16.7)	0.5±0.3 (83.3)	1.5±0.7 (57.7)	0.3±0.2 (60.0)
	$PM_{2.5}$	5.8±2.3	2.2±1.5 (91.7)	0.2±0.1 (33.3)	0.6±0.5 (99.0)	1.8±0.8 (69.2)	0.4±0.2 (80.0)
	PM_{10}	8.0±2.6	2.4±1.5	0.6±0.3	0.6±0.5	2.6±1.1	0.5±0.3

Atmos. Chem. Phys. Discuss., doi:10.5194/acp-2016-390, 2016
Manuscript under review for journal Atmos. Chem. Phys.
Published: 13 May 2016

Atmospheric Chemistry and Physics Discussions

857 **Table 2.** Statistical parameters of samples with air masses from ocean

Site	Date	Droplet mode sulfate ($\mu g\ m^{-3}$)	Percentage of sulfate in droplet mode (%)	T (℃)	RH (%)	P (hPa)	WS ($m\ s^{-1}$)	Low Cloud cover (%)
GZ	2010/5/8	7.4	61	27.5	82.0	997.1	1.9	70
	2010/5/12	11.1	65	25.0	77.5	1002.9	1.5	60
ZH	2010/5/12	9.5	67	24.9	83.0	1006.1	3.4	70
	2010/6/1	6.8	67	24.8	80.0	1002.0	5.1	70
JFM	2010/5/4	2.2	64	22.0	83.0	916.9	1.0	70
	2010/5/13	2.5	67	23.7	75.8	918.3	1.8	70

858